

## The lithosphere-asthenosphere boundary in the North-West of Iran from S receiver function

Taghizadeh-Farahmand, F.<sup>1\*</sup>, Sodoudi, F.<sup>2</sup>, Gheitanchi, M. R.<sup>3</sup> and Afsari, N.<sup>4</sup>

<sup>1</sup>Assistant Professor, Department of Physics, Qom Branch, Islamic Azad University, Qom, Iran

<sup>2</sup>Helmholtz Center Potsdam, GFZ Research Center for Geosciences, Telegrafenberg 14473 Potsdam, Germany

<sup>3</sup>Professor, Earth Physics Department, Institute of Geophysics, University of Tehran, Iran

<sup>4</sup>Ph. D. Student of Seismology, Islamshahr Branch, Islamic Azad University, Tehran, Iran

(Received: 14 Oct 2008, Accepted: 24 Jan 2009)

### Abstract

Recently, the S receiver function method has been successfully developed to identify upper mantle interfaces. S receiver functions have the advantage of being free of s-wave multiple reflections and can be more suitable than P receiver function for studying mantle lithosphere. However, because of specific ray geometry of the S-to-P converted waves, the S receiver function method has some technical difficulties and limitations. We selected data from teleseismic events ( $M_b > 5.7$ , epicentral distance between  $60^\circ - 85^\circ$ ) recorded since 1996 to present at 8 three component short period stations from the Tabriz Telemetry Network. Clear negative signals from the lithosphere-asthenosphere boundary (LAB) are observed. The average LAB depth is approximately 85 Km and varies from 77 to 103 km underneath the NW of Iran.

**Key words:** lithosphere- asthenosphere boundary, S receiver function, Teleseismic event, NW of Iran

### بررسی مرز سنگ کره – سست کره زیر شمال غرب ایران، به کمک تابع گیرنده S

فتانه تقی زاده فرهمند<sup>۱</sup>، فروغ صدودی<sup>۲</sup>، محمدرضا قیطانچی<sup>۳</sup> و نرگس افسری<sup>۴</sup>

<sup>۱</sup> استادیار، گروه فیزیک، دانشکده علوم دانشگاه آزاد اسلامی واحد قم، ایران

<sup>۲</sup> پژوهشگر، مؤسسه تحقیقاتی علوم زمین هلمهولتز، پتسدام، آلمان

<sup>۳</sup> استاد، گروه فیزیک زمین، مؤسسه ژئوفیزیک دانشگاه تهران، ایران

<sup>۴</sup> دانشجوی دکتری زلزله شناسی، دانشگاه آزاد اسلامی واحد اسلام شهر، تهران، ایران

(دریافت: ۱۳۸۷/۰۷/۲۳، پذیرش نهایی: ۱۳۸۷/۱۱/۱۵)

### چکیده

تابع گیرنده S ابزار مناسبی برای محاسبه ضخامت سنگ کره در هر منطقه است. سنگ کره سازنده صفحه های تکتونیکی زمین است. در بیشتر مکان ها، مرز سنگ کره و سست کره با مشاهدات سرعت های لرزه ای کم یا تغییرات منفی سرعت مشخص می شود. در این بررسی به کمک تحلیل تابع گیرنده S، با استفاده از زمان رسید تبدیل Sp در مرز سنگ کره – سست کره ضخامت سنگ کره محاسبه شد. مزیت استفاده از تابع گیرنده S در این است که فازهای تبدیلی Sp قبل از رسید مستقیم S و همه بازتاب های مربوطه و بازتاب های شان بعد از رسید مستقیم S در ایستگاه دریافت می شوند و شناسایی فاز تبدیلی Sp آسان تر است. در صورتی که این فاز تبدیلی در تابع گیرنده P با بازتاب های پوسته پوشیده می شود. به منظور محاسبه تابع گیرنده S ابتدا در صورت متفاوت بودن پاسخ بسامدی سه لرزه نگار در راستای E-W, N-S, Z، باید اثر دستگاهی از روی آنها حذف شود. سپس دو مؤلفه افقی (N-S, E-W) تحت زاویه Back Azimuth چرخانده شده و به جهات شعاعی و مماسی (R, T) تبدیل می شوند. در مرحله بعد چرخش دستگاه

\*Corresponding author: Tel: 0251-2933185 Fax: 021-28005797 E-mail: f\_farahmand@qom-iau.ac.ir

مختصات ZRT به دستگاه مختصات محلی پرتو LQT (P, SV, SH) صورت می‌گیرد. برای اجرای صحیح چرخش باید زاویه تابش صحیح انتخاب شود. برای این منظور، مؤلفه‌های L حول مجموعه‌ای از زوایای تابش چرخانده می‌شوند. زاویه‌ای که انرژی موج S در زمان رسیدش حداقل می‌شود تقریب خوبی از زاویه تابش درست است. بعد از مرحله چرخش، بیشتر انرژی فازهای تبدیلی Sp روی مؤلفه‌های L خواهد بود. به‌منظور حذف سیگنال S از مؤلفه‌های L، مؤلفه‌های L را با سیگنال S روی مؤلفه Q واهم‌آمیخت می‌کنیم. مؤلفه L حاصل که شامل فازهای تبدیلی Sp بدون بازتاب‌های چندگانه است را تابع گیرنده S می‌نامند. به دلیل وابستگی زمان رسید امواج تبدیل Sp به کندی موج S باید تصحیح دینامیکی روی توابع گیرنده S صورت گیرد. از آنجا که تبدیلات Sp عموماً ضعیف‌اند، برای بهبود نسبت سیگنال به نوفه، بعد از اعمال تصحیح دینامیکی، توابع گیرنده S را با هم جمع می‌کنیم. در نهایت با تبدیل اختلاف زمانی بین فازهای تبدیلی و موج S مستقیم به عمق با استفاده از مدل سرعتی مرجع IASP91 می‌توان عمق ناپیوستگی‌ها را به‌دست آورد. برای این منظور داده‌های زمین‌لرزه‌های دورلرز ثبت شده ۸ ایستگاه ثابت دوره کوتاه شبکه دورلرز تبریز در شمال غرب ایران از ۱۹۹۵ تا ۲۰۰۸ با بزرگای  $M_b \geq 5.7$  و در فاصله رو مرکزی  $85^\circ < \Delta < 60^\circ$  مورد پردازش قرار گرفت. مقدار ضخامت LAB به‌طور متوسط ۸۵ کیلومتر محاسبه شد و مقدار آن از ۷۷ کیلومتر زیر غربی‌ترین ایستگاه شبستر (SHB)، تا ۱۰۳ کیلومتر زیر شرقی‌ترین ایستگاه سراب (SRB)، در تغییر بود.

واژه‌های کلیدی: تابع گیرنده S، مرز سنگ‌کره-سست‌کره، دورلرز، شمال غرب ایران

## 1 INTRODUCTION

The thickness of the lithosphere, the cold boundary layer near the earth's surface, controls the heat loss and tectonics of oceans and continents (Priestley and McKenzie, 2006). Once plate tectonics had been generally accepted, it became clear that the properties of the entire lithosphere beneath cratons were likely to be responsible for their behaviour rather than those of the crust alone (McKenzie and Priestley, 2007). The lithosphere is generally divided into two parts. The crust lithosphere includes the upper part of the lithosphere, whereas the mantle lithosphere located in the lower part moves as the high velocity lid on the top of the asthenosphere. The high viscosity lithospheric plates moving over a lower viscosity asthenosphere is a basic element of plate tectonics. Observations of low seismic velocities in the upper mantle are generally associated with the lithosphere-asthenosphere boundary named LAB. This boundary appears as a negative contrast in which the seismic velocities decrease with depth. In contrast to the Moho depth which is usually observed at high resolution by different techniques such as the P receiver function method, the lower boundary of the mantle lithosphere is generally considered not sharp enough to be well observed by seismic body wave observations. The thickness of the

lithosphere has been mostly obtained from low resolution surface wave observations. The lithosphere has a global average thickness of 80-100 km, ranging between zero and 200 km beneath mid ocean ridges and stable cratons, respectively (Kumar et al., 2005a). However, the recently developed S receiver function technique (Li et al., 2004; Kumar et al., 2005a; Sodoudi et al., 2006 a,b) can be optimally used to identify the LAB boundary using higher resolution body waves, since this method is free of multiples. This boundary is almost invisible in the P receiver function due to the crustal multiples, which arrive at the same time and heavily disturb the time window of the LAB arrival. The thickness of the lithosphere is one of the most important parameters to address the problems of the plate tectonic processes.

The main goal of this paper is to derive a more homogeneous image of the lithosphere-asthenosphere boundary for NW of Iran. To obtain this goal, we use the S receiver function method.

## 2 TECTONIC SETTING OF NW IRAN RECIION

Iran is located as a part of the Alpine-Himalayan orogenic belt. The region referred to in this study as northwest Iran is enclosed

between 45°-48° east longitude and 37°-39° north latitude (figure 1). This region is one of the seismologically active regions in the Middle-East and has experienced many destructive earthquakes (Gheitanchi et al., 2004). This area appeared with the closure of the Neotethys Ocean and with the collision of the Arabian plate and the central Iran block and deformation. NW Iran is a region of intense deformation and seismicity situated between two thrust belts of the Caucasus to the north and the Zagros mountains to the south (Hessami et al., 2006). Deformation and seismicity in this region is mainly due to the continental shortening between the Eurasian and Arabian plates. Geological evidences and fault plane solutions of earthquakes in this region indicate the existence of both thrust and conjugate strike-slip faulting (Jackson, 1992). Several NW-SE trending major faults such as the Tabriz fault and the Bostanabad fault are examples of well known major faults in northwest Iran. A group of N-S trending minor faults is observed around Tabriz and extended to the North. Another minor fault system with NE-SW trend, almost perpendicular to the north Tabriz major fault, is observable from the

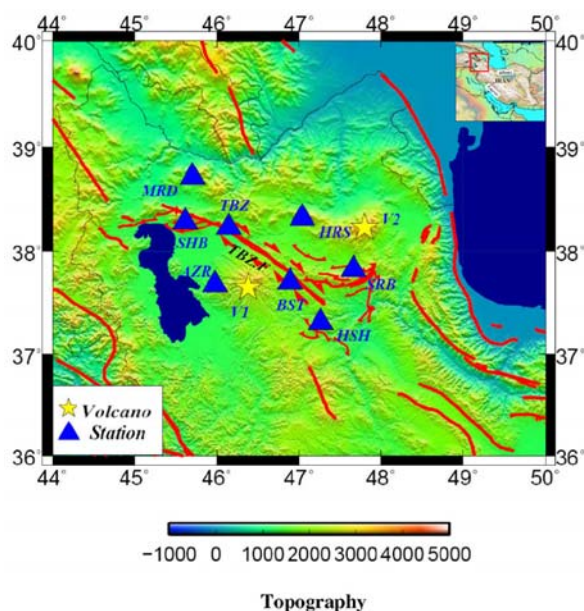
northeast part of Ardabil, passing through Meshghinshahr and Azarshahr and crossing Orumiye lake as well as the Orumiye the major fault in west extreme (Gheitanchi et al., 2004). More groups of faults with different trends are indicating a complicated pattern of deformation in northwest Iran.

### 3 DATA AND METHOD OF STUDY

#### 3-1 DATA

We selected teleseismic events ( $M_b > 5.7$ ,  $60^\circ < \Delta < 85^\circ$ ) recorded from 1996-2007 at 8 three component stations from the permanent Tabriz Telemetry Network (AZR, BST, HRS, HSH, MRD, SHB, SRB and TBZ). These stations are equipped with SS-1 seismometers with frequency response of 1 Hz made by Kinometrics Co., VHF antenna, Tx transmitters made by Nanometrics of Canada, 16-bit digitizers, and a power supply based on solar energy. The data is recorded on a 50-samples-per-second. Figure 1 shows the setup of the Tabriz Telemetry Network and table 1 lists station names and coordinates.

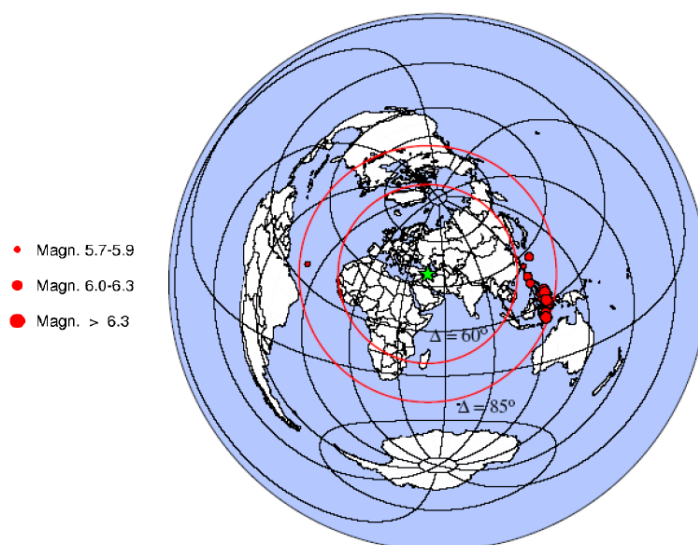
Figure 2 shows teleseismic events which are used in the study.



**Figure 1.** Location map of the seismological stations (triangle) used in this study. The main faults are shown by the red lines.

**Table 1.** Specification of the seismic stations shown in figure 1.

Station name	Station code	Latitude (Deg.)	Longitude (Deg.)	Elevation (m)
Azarshahr	AZR	37.6783	45.9800	2300
Bostanababd	BST	37.7000	46.8917	2100
Hashtroud	HSR	37.3067	47.2633	2850
Heris	HRS	38.3183	47.0417	2100
Marand	MRD	38.7133	45.7033	1684
Sarab	SRB	37.8250	47.6667	1950
Shabestar	SHB	38.2833	45.6166	2150
Tabriz	TBZ	38.2333	46.1466	1650

**Figure 2.** The epicenter distribution of events used to determine S receiver functions. The green star shows the center of the Tabriz Telemetry Network. The red solid circles mark the 60° and 85° epicentral distances, respectively.**Table 2.** List of events recorded by Tabriz Telemetry Network for S receiver function.

Time	Date	Lat (Deg.)	Lon (Deg.)	Depth (km)	M <sub>b</sub>	Epicentral Distance (Deg.)
1996 2 28	9 44 10.9	1.756	126.048	115	6.2	80.66
2001 1 1	6 57 4.17	6.898	126.579	33	6.4	77.92
2002 3 5	21 16 9.13	6.033	124.249	31	6.3	76.61
2002 12 30	4 49 8.69	7.471	123.407	10	5.9	75.07
2003 5 5	23 4 45.7	3.715	127.954	56	6	80.95
2003 5 5	15 50 8.47	0.215	127.354	123	5.9	82.64
2003 5 26	23 13 29.7	6.761	123.707	565	6.2	75.74
2003 5 26	23 26 31.9	6.812	123.88	583	5.9	75.85
2003 11 12	0 29 45.4	1.593	126.48	33	5.7	81.10
2004 6 30	23 37 25.5	0.797	124.726	90	6	80.22
2005 1 20	16 47 1.86	3.739	126.814	10	5.9	80.04
2005 2 15	14 42 25.9	4.756	126.421	39	6.1	79.10
2005 3 4	19 5 19.9	2.67	126.407	59	6.1	80.38
2006 3 31	21 14 47.2	3.787	126.369	54	5.9	79.66
2007 6 16	1 18 47.9	1.152	126.413	47	5.8	81.30
2007 9 13	9 48 45.1	3.801	126.342	26	6.1	79.71

### 3-2 METHOD OF STUDY

S-to-P conversions produced at significant velocity discontinuities beneath the station (figure 3) can be obtained by deconvolving the Sv component from the P component. The S receiver functions have a significant advantage over P receiver functions because the converted Sp phase arrives earlier than the direct S phase (e.g., Faber and Müller, 1980; Bock, 1991; Farra and Vinnik, 2000; Li et al., 2004; Kumar et al., 2005a; Sodoudi et al., 2006a) and therefore upper mantle conversions are free from interface of crustal multiples (figure 4, right panel). The converted Sp phases are generally best observed at epicentral distances between 60° and 85° (Faber and Müller, 1980).

Since the time difference between converted Sp and S waves depends on the ray parameter, we correct the S-to-P conversions to a common distance using a reference slowness of  $6.4 \text{ sdeg}^{-1}$ . Although this value is not necessarily realistic for S waves, it is used to make P and S receiver function timescales directly comparable. The S receiver functions are much noisier than P receiver functions due to their later arrival times. They also have a longer periods in comparison with the P receiver functions and resolve less fine structure within the crust and mantle lithosphere. However, the fact that they are free multiples enables the identification of Sp conversions at mantle

discontinuities. Therefore, mantle discontinuity conversions, which are masked by crustal multiples arriving at nearly the same time in P receiver functions, can be isolated in the S receiver function (figure 4).

Figure 4 demonstrates a simple two layered model over a half space containing crust-mantle and lithosphere-asthenosphere boundaries at about 30 and 125 km, respectively. The synthetic P and S receiver functions are computed and compared. The P onset (for P receiver function) and S onset (for S receiver function) are fixed to be on zero. While the Ps converted phase arrives later than the direct P phase, the converted Sp phase is a precursor of the direct S wave and arrives earlier. As figure 2 shows, all multiples arrive after the direct S wave, therefore they cannot disturb the major conversions. The computed P receiver function shows the converted Ps phase at Moho as well as its multiples. The converted phase from lithosphere-asthenosphere boundary is covered by the multiples arriving at the same time on the S receiver function at 13s (reversed time). Assuming the same ray parameter, the arrival time of the converted Sp phase at Moho is similar to that of the P receiver function but in the reversed time (3.5s). Different sign of the S-to-P conversion coefficient relative to those of P-to-S conversion makes a reversed polarity for the Sp converted phase.

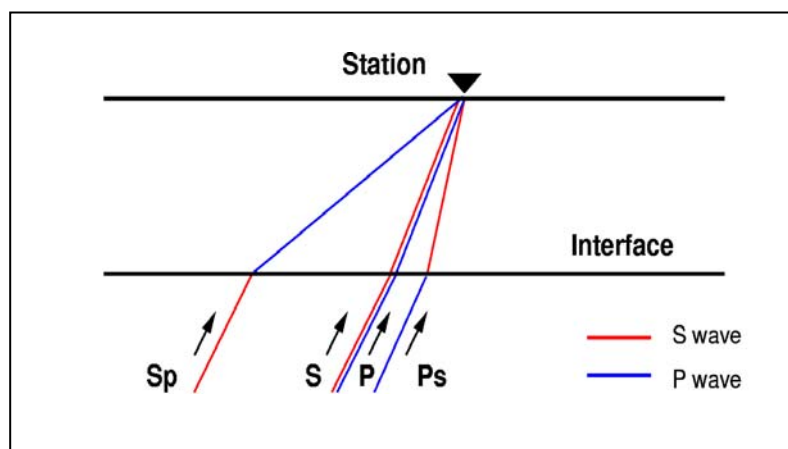
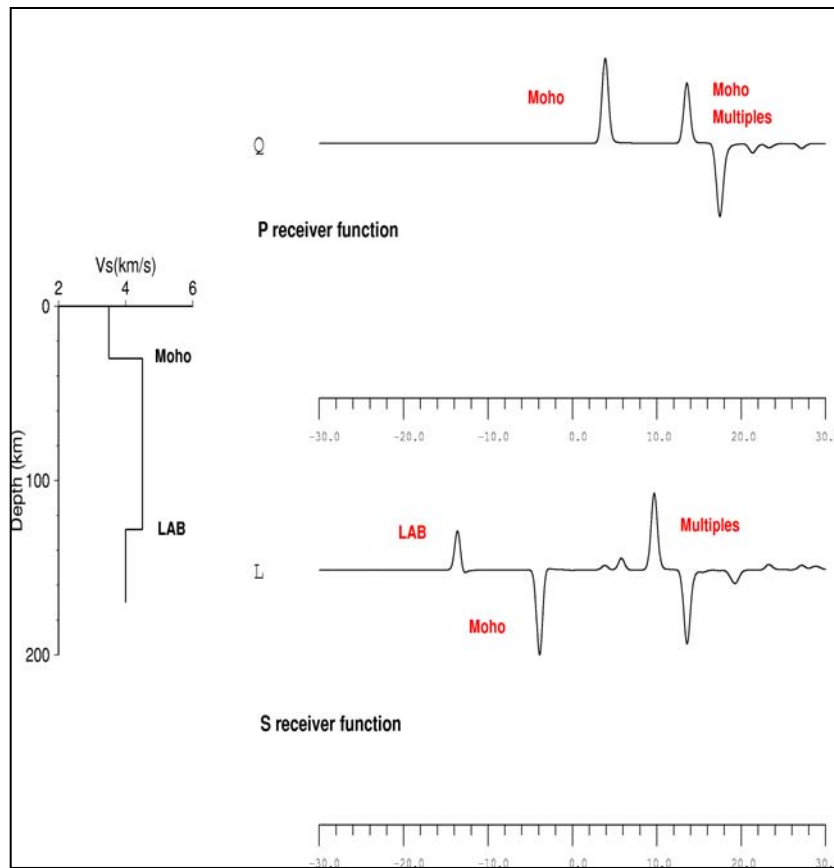


Figure 3. Ray path of P and S waves.



**Figure 4.** Synthetic P and S receiver functions are computed for a two layered model over a half space shown in the left part of the figure.

#### 4. DISCUSSION AND CONCLUSION

In this study, we selected a time window of 200 seconds in length (100s before the S onset) and calculated the S receiver function by applying band pass filter 4-20 s. Calculation of S receiver function includes mainly coordination rotation and deconvolution. We rotated the ZNE components into the LQT system using back azimuth and incidence angle. The angle of incidence is defined by the minimum of energy in the L component at arrival time of the S phases. As an example, the figure 5 represents an event at  $81^\circ$  epicentral distance with magnitude of 5.7 recorded at short period station AZR. The figure shows the L components obtained from rotation around incidence angles of  $0-72^\circ$ . The best observed incidence angle is indicated with a red arrow ( $27^\circ$ ) and the amplitude of the LAB

converted phase occurred about 11 s. Prior stacking, the moveout correction for reference slowness of  $6.4 \text{ sdeg}^{-1}$  (IASP91 global reference model) was applied. To make the S receiver functions look like conventional P receiver functions, we reversed the polarity of the S receiver function amplitudes as well as the time axis. The S receiver functions for some stations are shown in figure 6. Negative amplitudes are plotted in gray indicate velocity decreasing downwards, while positive amplitudes in red show an increasing velocity with depth (Sodoudi, 2005). The S receiver functions are sorted by their back azimuth. The phase is visible on the record, which is marked on the summation trace at the top in figure 6 with negative amplitude ranging between 8.5-11.5s delay time, indicating the converted Sp phase due to the lithosphere-asthenosphere boundary (labeled with LAB).

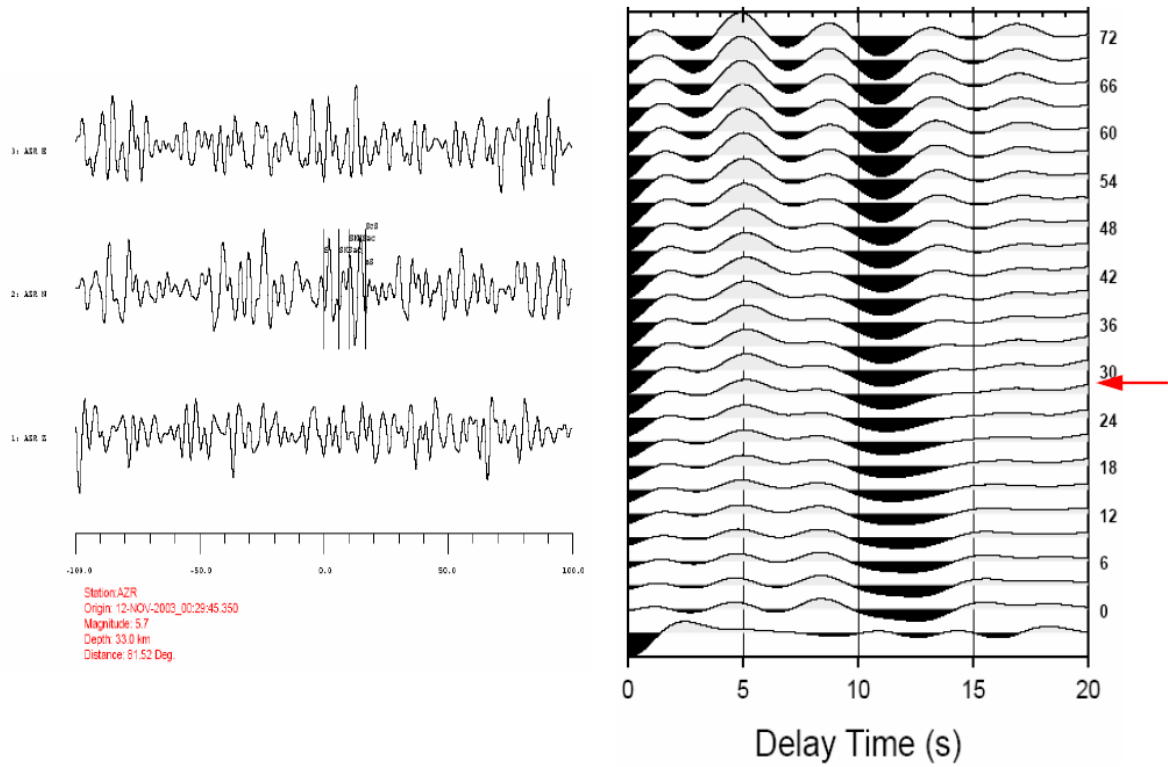


**Figure 5.** The L component has been rotated around different incidence angles ranging between 0-72°. The observed incidence angle is indicated with the red arrow. The left part is the parameters of the event.

The delay times of the LAB phase obtained from each station were converted into the depth. The arrival times of the LAB in seconds may be multiplied by factor of 9 (according the IASP91 reference model) to obtain the LAB depth estimate in kilometers. Delay times and depth values of the NW Iran are given in table 2.

To generate a depth section, the receiver functions for each station is migrated. In the migration process, each single receiver function is back-project along its path. The

paths are calculated using IASP91 reference model (Kennett and Engdahl, 1991). The obtained 2D migrated section along the longitude is represented in figure 7. Positive amplitudes of receiver functions are plotted in red (Moho), while negative amplitudes are in blue (LAB). The converted phase associated with the LAB is observed under network at about 80 km. The obtained 2D migrated section confirms our results that were computed from S receiver functions.

**Table 2.** The Sp conversion times and depth of LAB.

Station	AZR	BST	HSH	HRS	MRD	SRB	SHB	TBZ
Delay time (s)	11.2	8.5	8.6	8.6	9	11.5	8.5	8.6
Depth (Km)	101	77	78	78	81	103	77	78

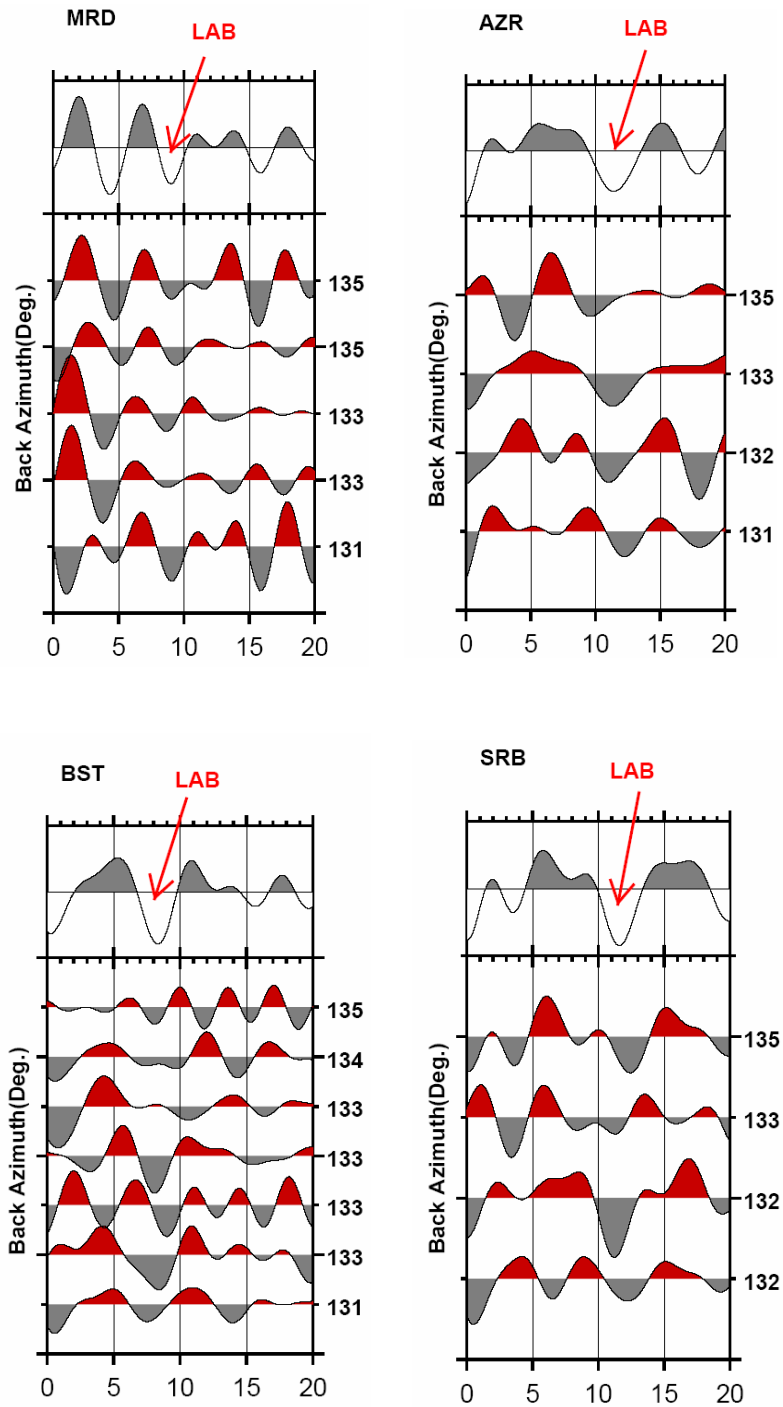


**Figure 6.** Individual S receiver functions for some stations in the Tabriz network are sorted by their back azimuth. Negative amplitudes are plotted in gray and indicate velocity decreasing downwards. The S receiver functions are plotted in reverse time in order to compare with P receiver functions. The arrows on the stacked trace show the average time of the Sp conversions generated by the lithosphere-asthenosphere boundary.

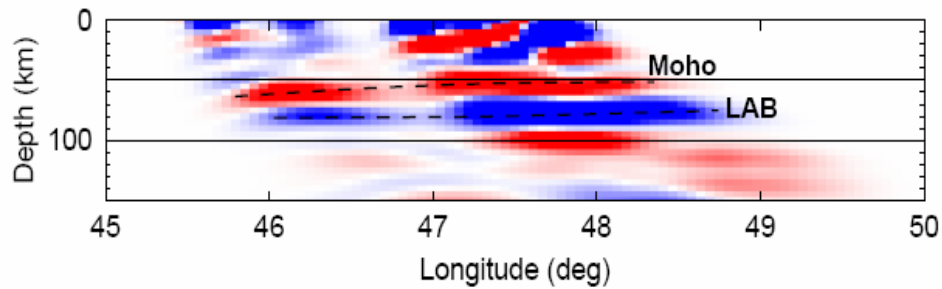


**Figure 7.** The 2D migrated S receiver function section along the longitude. The positive (negative) amplitudes of the receiver function are plotted in red (blue). The LAB lies at about 80 km.

Unlike P receiver functions, the Sp conversions are not located close to the stations and show additionally significant overlapping with the Sp conversions obtained from adjacent stations. In figure 8 the location of the piercing points at 100 km depth (likely to be approximately the thickness of the LAB) for the Sp conversions are plotted. The locations of piercing points of S receiver functions at 100 km depth are indicated by cross marks. Since the Sp conversions are generally weak, a stacked S receiver function was computed based on the

latitude and longitude of the piercing points. In figure 9 the computed stacked S receiver functions for piercing points at 100 km depth are plotted. The stacking method enhances the conversions and reduces the error of the depth determination by averaging the information of several single traces within each station. Negative (positive) amplitudes, plotted in gray (black) indicate a velocity decrease (increase) with depth. A clear negative phase (labeled LAB) at  $\sim 8.7s$  is apparent.

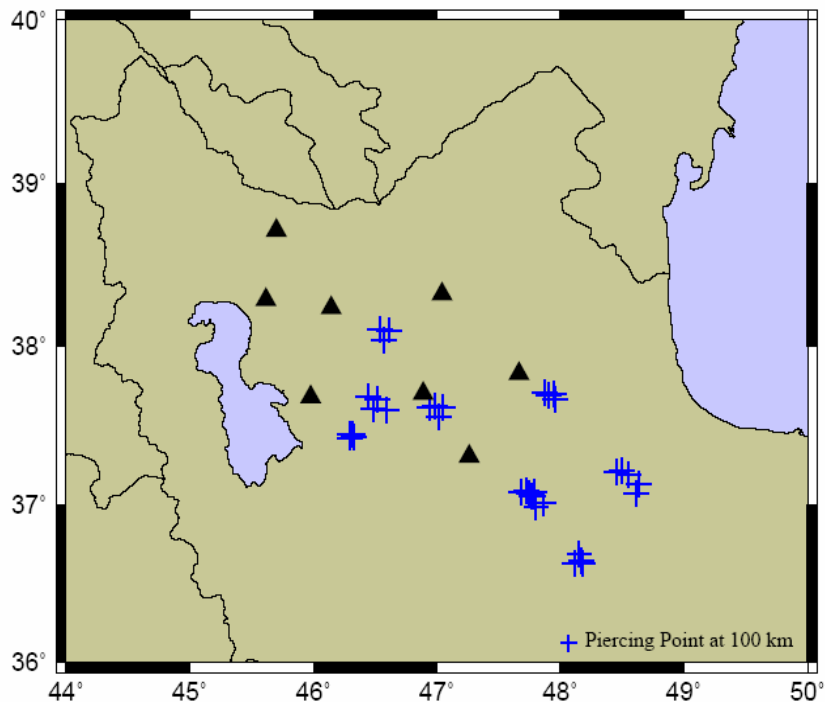


**Figure 8.** Location of piercing points (blue crosses) of S receiver functions at 100 km depth. Stations are indicated by black triangles.

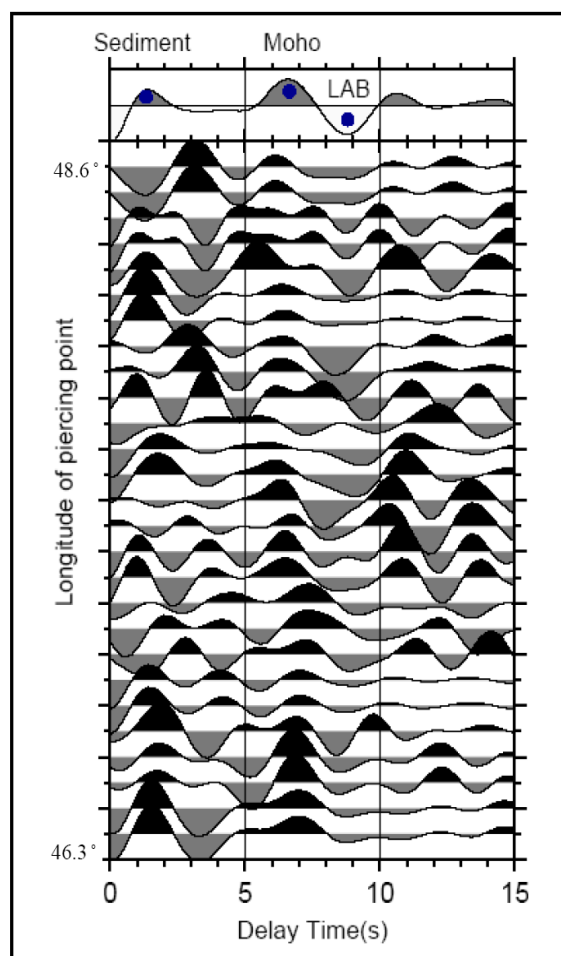


**Figure 9.** The stacked S receiver functions are computed based on latitude and longitude of piercing points. Negative (positive) amplitudes, plotted in gray (black) indicate a velocity decrease (increase) with depth. A clear negative phase (labeled LAB) at  $\sim 8.7$  is labeled on the summation trace.

In this study, we use short period data to obtain S receiver functions. The Moho Ps conversions ( $\sim 6$ s) in S receiver functions are in good agreement with Moho depth obtained from P receiver functions (T-Farahmand et al, 2008). According to the error introduced by the selected reference velocity model IASP91 ( $\sim 5$ -10 km), our results are expectable. These results are also in good agreement with other geophysical studies in this region (Priestley and McKenzie, 2006; McKenzie and Priestley, 2007).

The lithosphere–asthenosphere boundary is not completely flat in NW Iran. The S receiver function obtained from a short period seismograms map a clear LAB

showing a thin continental lithospheric thickness of 85 Km and varies from 77 to 103 km. Deeper and shallower lithosphere–asthenosphere boundary are found under the western and eastern parts beneath SHB and SRB stations respectively.

## 6 ACKNOWLEDGMENTS

Authors are grateful to the Institute of Geophysics, University of Tehran for preparing the teleseismic waveforms. We used the software packages SeismicHandler for data processing and GMT for plotting, respectively.

## REFERENCE

- Bock, G., 1991, Long-period S to P converted waves and the onset of partial melting beneath Oahu, Hawaii. *Geophys. Res. Lett.*, **18**, 869-872.
- Faber, S. and Müller, G., 1980, Sp phases from the transition zone between the upper and lower mantle, *B. Seismol. Soc. Am.*, **70**, 487-508.
- Farra, V. and Vinnik, L., 2000, Upper mantle stratification by P and S receiver functions, *Geophys. J. Lett.*, **141**, 699-712.
- Gheitanchi, M. R., Mirzaei, N. and Bayramnejad, E., 2004, Pattern of seismicity in Northwest Iran, Revealed from local seismic network, *Geosci.*, **11**, 104-111.
- Hessami, K., Pantosti, D., Tabasi, H., Shabaniyan, E., Abbasi, M. R., Fegghi, K., and Soleymani, S., 2006, Paleoearthquakes and slip rates of the North Tabriz Fault, NW Iran: preliminary results, *Ann. Geophys.*, **64**, 903-915.
- Jackson, J., 1992, Partitioning of strike-slip and convergent mountain between Eurasia and Arabia in Eastern Turkey and the Caucasus, *J. Geophys. Res.*, **97**, 471-479.
- Kennett, B. L. N., Engdahl, E. R., 1991, Travel times for global earthquake location and phase identification, *Geophys. J. Int.*, **105**, 429-465.
- Kumar, P., Kind, R., Hanka, W., Wylegalla, K., Reiber, Ch., Yuan, X., Wolbern, I., Schwintzer, P., Fleming, K., Dahl-Jensen, T., Larsen, T., Schweitzer, J., Priestly, W., Gudmundsson, O., and Wolf, D., 2005a, The lithosphere-asthenosphere boundary in the North-West Atlantic region, *Earth Planet. Sci. Lett.*, **236**, 249-257.
- Kumar, P., Kind, R., and Kosarev, G., 2005b, The lithosphere-asthenosphere boundary in the Tien Shan-Karakoram region from S receiver functions: Evidence for continental subduction, *Geophys. Res. Lett.*, **32**, L07305.
- Li, X., Kind, R., Yuan, X., Wolbern, I. and Hanka, W., 2004, Rejuvenation of the Lithosphere by the Hawaiian plume, *Nature*, **427**: 827-829.
- McKenzie, D., Priestley, K., 2007, The influence of lithospheric thickness variations on continental evolution, *Lithos.*, **01584**, 11p.
- Priestley, K., McKenzie, D., 2006, The thermal structure of lithosphere from shear wave velocities, *Earth Planet. Sci. Lett.* **244**, 285-301.
- Sodoudi, F., 2005, Lithospheric structure of the Aegean obtained from P and S receiver functions, FU Berlin, PhD thesis, 167pp.
- Sodoudi, F., Kind, R., Priestley, W., Hanka, W., Wylegalla, K., Stavrakakis, G., Vafidis, A., Harjes, H. P., and Bohnhoff, M., 2006a, Lithospheric structure of the Aegean obtained from P and S receiver functions, *J. Geophys. Res.*, **11**, 12307-12330.
- Sodoudi, F., Yuan, X., Liu, Q., Kind, K., and Chen, J., 2006b, Lithospheric thickness beneath the Dabie Shan, central eastern China from S receiver functions, *Geophys. J. Int.*, doi:10.1111/j.1365-246X.2006.03080.X.
- Taghizadeh-Farahmand, F., Sodoudi, F., Gheitanchi, M. R. and Kaviani, A., 2008, Crustal structure beneath Northwest Iran using teleseismic converted waves, *J. Earth Sci. (GSI)*, **68**, In press.